Z. Phys. A 346, 253–260 (1993)

ZEITSCHRIFT
FÜR PHYSIK A

M1 resonances in unstable magic nuclei

S. Kamerdzhiev *, J. Speth **, G. Tertychny *, J. Wambach ***

Institut für Kernphysik, Forschungszentrum Jülich, Postfach 1913, D-52425 Jülich, Germany

Received: 10 March 1993 / Revised version: 2 June 1993

Abstract. Within a microscopic approach which takes into account RPA configurations, the single-particle continuum and more complex $1p1h\otimes phonon$ configurations isoscalar and isovector M1 excitations for the unstable nuclei ^{56,78}Ni and ^{100,132}Sn are calculated. For comparison, the experimentally known M1 excitations in ^{40}Ca and ^{208}Pb have also been calculated. In the latter nuclei good agreement in the centroid energy, the total transition strength and the resonance width is obtained. With the same parameters we predict the magnetic excitations for the unstable nuclei. The strength is sufficiently concentrated to be measurable in radioactive beam experiments. New features are found for the very neutron rich nucleus ^{78}Ni and the neutron deficient nucleus ^{100}Sn.

PACS: 21.10.−k; 21.60.−n; 24.30.Cz

1. Introduction

There is a rich history in the study of $M1$ excitations in nuclei (see [1] for a recent review). For more than two decades the experimental effort has concentrated on stable nuclei. Unfortunately, this greatly limits the number of accessible magic nuclei which, because of their simple shell structure, may exhibit strong $M1$ transitions between spin-orbit partners. With the availability of radioactive beam facilities this may change since far from stability new magic nuclei become available [2]. Thus one can hope to obtain a more systematic understanding of the residual interaction, the renormalization of the magnetic operator and the damping mechanisms of $M1$ resonances. Besides, such nuclei are also of astrophysical interest (see references in [3]).

The aim of the present paper is to extend the microscopic models which describe well the known resonances to the new region accessible by radioactive beams. As is well known, the RPA with phenomenological Landau-Migdal interactions is able to reproduce the excitation energies of known isoscalar and isovector $M1$ excitations with a universal set of spin-interaction parameters g and g' (some caution should be exercised in terming a transition isoscalar or isovector since there is some well-known mixing between the two). Including effective spin g-factors $\sim 0.7-0.8$ the observed total transition strengths are also reproduced [4–7]. The RPA fails, however, to account for the resonance width which, especially in heavy nuclei, is caused by a coupling to more complex configurations. For the $M1$ case there are several approaches for including such configurations [8–10]. Concerning the quenching of $M1$ strength the most reliable approach seems to be the use of phenomenological values for the g-factors. By now, these are very well establish from a variety of experiments [7, 11] and are universal for all nuclei measured. For predictions in unstable nuclei knowledge of global interaction parameters and g-factors is of crucial importance.

Most realistically, the more complex configurations are described as one-particle one-hole states coupled to low-lying surface vibrations ($1p1h\otimes phonon$ states) using known parameters. Recently a formalism for including such configurations in conjunction with the single-particle continuum has been successfully used in the description of giant electric resonances [12, 13]. In particular, the widths are reproduced satisfactorily. We shall employ this approach here in the study of $M1$ transitions in unstable nuclei.

The theory will be briefly described in Sect. 2. In Sects. 3 and 4 calculations for the known $M1$ states in ^{48}Ca and ^{208}Pb are presented which show the quality of the theoretical results. The same interaction parameters, effective charges and a standard mean field of the Woods-Saxon type are then used to predict spectra for unstable nuclei.

* *Permanent address:* Institute of Physics and Power Engineering, 249020 Obninsk, Russia

** Also at: Institut für Theoretische Kernphysik, Nußallee 14–16, D-53115 Bonn, Germany

*** Also at: Department of Physics, University of Illinois at Urbana-Champaign, Urbana, IL 61801, USA

2. Theory

The approach which we shall use has been developed in the framework of the consistent Green's function method and is based on Migdal's Theory of Finite Fermi Systems (TFFS) [14]. The main physical idea is to include $1p\,1h\otimes$ *phonon* configurations instead of "pure" $2p\,2h$ ones and thus to make use of the fact that, in magic nuclei, the squared phonon creation amplitude is a small parameter $g^2<1$. This enables one to restrict the calculation to particle-phonon coupling terms of order g^2. Furthermore only a small number of phonons of maximum amplitude (maximal g^2) need to be considered, i.e. the most collective low-lying ones. This makes it possible to use known parameters of the TFFS which determine the local effective interaction and quasiparticle charges (taking phonons into account explicitly gives non-local contributions). In addition, a small number of phonons greatly reduces the computational effort. This physical assumption has been confirmed in several calculations of $M1$ excitations [10], the giant dipole resonance [12, 13] as well as $E2$, $E0$ resonances [15].

The theory is formulated, most efficiently, in coordinate space. For an applied external field V^0 with frequency ω, the change in density $\delta\rho=\rho-\rho_0$ from equilibrium is given by

$$\delta\rho(\mathbf{r},\omega)=-\int \mathrm{d}\mathbf{r}'\,A(\mathbf{r},\mathbf{r}',\omega)(e_q\,V^0(\mathbf{r}')+\mathscr{F}(\mathbf{r}')\,\delta\rho(\mathbf{r}',\omega)) \quad (1)$$

and the frequency distribution determines the excitation spectrum of the system. Here e_q denotes the local quasiparticle charge and $\mathscr{F}$ the quasiparticle interaction. As discussed above, these can be taken from the TFFS. The generalized propagator A contains the RPA part as well as the $1p\,1h\otimes$ *phonon* configurations and was derived in [16] in a representation of the discrete single-particle basis $\{\tilde{\phi}_\lambda,\tilde{\varepsilon}_\lambda\}$. The tilde indicates that these states have been corrected for mean field contributions from the particle-phonon coupling, already included in phenomenological potentials of the Woods-Saxon type. Since these contributions are included explicitly they have to be removed from the single-particle potential to avoid double counting. To include single-particle emission, the discrete propagator A_{1234} has to be augmented by a continuum part and takes the form

$$\begin{aligned}A(\mathbf{r},\mathbf{r}',\omega)=&\tilde{A}^{\mathrm{RPA}}_{\mathrm{cont}}(\mathbf{r},\mathbf{r}',\omega)\\&+\sum_{1234}[A_{1234}(\omega)-\tilde{A}^{\mathrm{RPA}}_{1234}(\omega)\,\delta_{13}\,\delta_{24}]\\&\cdot\,\tilde{\phi}^*_1(\mathbf{r})\,\tilde{\phi}_2(\mathbf{r})\,\tilde{\phi}_3(\mathbf{r}')\,\tilde{\phi}^*_4(\mathbf{r}')\end{aligned} \quad (2)$$

where $\tilde{A}^{\mathrm{RPA}}_{\mathrm{cont}}$ is the continuum RPA propagator (for details see [17, 18]).

The $M1$ transition probabilities between the ground- and excited states are determined by the strength function

$$\frac{\mathrm{d}B(M1)}{\mathrm{d}\omega}=\sum_n|\langle n|e_q\,V^0|0\rangle|^2\,\delta(\omega-\omega_n). \quad (3)$$

Via the optical theorem this is related to $\delta\rho$ as

$$\frac{\mathrm{d}B(M1)}{\mathrm{d}\omega}=-\frac{1}{\pi}\,\mathrm{Im}\int \mathrm{d}\mathbf{r}\,e_q\,V^0(\mathbf{r})\,\delta\rho(\mathbf{r},\omega) \quad (4)$$

and the solutions of (1) determine $\mathrm{d}B(M1)/\mathrm{d}\omega$.

The summation over single-particle states in (2) is usually performed for two shell above and below the Fermi level. Aside from providing a finite width above the continuum threshold our method has the distinct advantage, over discretized calculations of this type, that the matrix dimension still remains manageable.

A major difference between the approach presented above and similar approaches [19–21] is the consistent inclusion of ground state correlations (GSC) beyond the RPA. There are two kinds of such $2p\,2h$ (to be more exact $1p\,1h\otimes$ *phonon* in our case) correlations. One is GSCs without "backward going" diagrams containing the quasiparticle-phonon interaction. The second one which includes these diagrams has new contributions which generate new transitions. In the RPA, GSCs are caused by non-pole diagrams, only, which cannot produce additional excited states. In this sense our theoretical extension is qualitatively different from the RPA. For $M1$ excitations in magic nuclei the consequences have been discussed in [10, 22] without taking into account the single-particle continuum. For the spin-saturated nuclei ^{16}O and ^{40}Ca, where strong $M1$ excitations are not allowed because of missing spin-orbit partners, one obtains $M1$ excitations which describe the experimental data reasonably well.

3. Approximations and parameters

The main physical approximations have been described above and in [12, 13]. Here we present the parameters used for the present calculations.

According to the selection rules only the spin-dependent part of the Landau-Migdal interaction

$$\mathscr{F}=C_0(g+g'\boldsymbol{\tau}\cdot\boldsymbol{\tau}')\,\boldsymbol{\sigma}\cdot\boldsymbol{\sigma}'\,\delta(\mathbf{r}_1-\mathbf{r}_2) \quad (5)$$

enters in the $M1$ excitations. In order to predict the $M1$ states in the unstable nuclei reliably we have slightly adjusted the g' parameter to obtain the well-known 1^+ levels in ^{48}Ca. This gives $g'=0.86$ instead of $g'=0.96$ used previously [7, 10, 16, 22] ($C_0=300$ MeV fm^3). For the parameter g we have used $g=-0.05$.

The local quasiparticle charge was determined from [14]

$$\begin{aligned}e^p_q\,V^{0p}&=(1-\xi_l)\,\mathbf{j}^p+[(1-\xi_s)\,\gamma^p+\xi_s\,\gamma^n+1/2\,\xi_l-1/2]\,\boldsymbol{\sigma}^p\\e^n_q\,V^{0n}&=\xi_l\,\mathbf{j}^n+[(1-\xi_s)\,\gamma^n+\xi_s\,\gamma^p-1/2\,\xi_l]\,\boldsymbol{\sigma}^n\end{aligned} \quad (6)$$

where $\gamma^p=2.79\,\mu_0$, $\gamma^n=-1.91\,\mu_0$, $\mu_0=e\hbar/2m_p c$ and

$$\xi^p_s=\xi^n_s=0.1,\qquad \xi^p_l=\xi^n_l=-0.03 \quad (7)$$

as obtained earlier [7, 10, 16, 22, 23]. These values yield for the spin local charge $e^p_q=0.64\gamma^p$ and $e^n_q=0.74\gamma^n$.

Table 1. Characteristics of the low-lying phonons used in the calculations

J^π	E, MeV	$B(EL)\uparrow$, e^2 fm^{2L}	J^π	E, MeV	$B(EL)\uparrow$, e^2 fm^{2L}	J^π	E, MeV	$B(EL)\uparrow$, e^2 fm^{2L}
^{100}Sn			^{132}Sn			^{48}Ca		
2^+	2.86	331	2^+	4.06	942	2^+	3.83	81.6
3^-	3.56	$5.33\ 10^3$	3^-	4.34	$5.0\ 10^4$	3^-	4.50	$1.12\ 10^4$
3^-	5.03	$5.99\ 10^3$	5^-	4.91	$3.46\ 10^6$			
5^-	3.57	$2.29\ 10^7$	5^-	5.61	$5.07\ 10^6$			
4^+	3.70	$1.02\ 10^5$	5^-	6.06	$5.43\ 10^6$			
4^+	4.09	$1.68\ 10^5$	5^-	6.85	$2.10\ 10^7$			
6^+	3.90	$9.16\ 10^7$	4^+	4.24	$1.80\ 10^6$			
6^+	4.81	$2.65\ 10^9$	6^+	4.75	$1.14\ 10^9$			
6^+	6.47	$6.36\ 10^8$	6^+	5.42	$1.06\ 10^9$			
6^+	6.79	$1.50\ 10^9$						
^{56}Ni			^{78}Ni			^{208}Pb		
2^+	2.73	361	2^+	3.53	1.45	3^-	2.61	$3.44\ 10^5$
3^-	4.62	$1.28\ 10^4$	4^+	3.70	$8.28\ 10^4$	2^+	4.07	$2.33\ 10^3$
5^-	6.35	$2.90\ 10^6$	4^+	4.67	$6.52\ 10^4$	2^+	9.71	$3.30\ 10^3$
4^+	3.73	$2.27\ 10^5$	4^+	4.99	$4.26\ 10^4$	4^+	4.34	$6.64\ 10^6$
6^+	5.18	$1.36\ 10^8$	6^+	4.00	$2.32\ 10^6$	6^+	4.40	$1.64\ 10^{10}$
			6^+	4.94	$4.17\ 10^7$	5^-	3.20	$2.60\ 10^8$
			3^-	4.38	$8.32\ 10^3$	5^-	3.70	$9.87\ 10^7$
			5^-	5.04	$1.18\ 10^6$			

Table 2. The single-particle levels for the unstable nuclei used in the calculations

nlj	^{132}Sn		^{100}Sn		nlj	^{56}Ni		^{78}Ni	
	n	p	n	p		n	p	n	p
$1s\,1/2$	−37.36	−39.49	−45.81	−29.52	$1s\,1/2$	−44.34	−37.19	−35.05	−41.39
$1p\,3/2$	−33.02	−34.78	−39.81	−24.33	$1p\,3/2$	−33.68	−26.12	−28.73	−34.73
$1p\,1/2$	−31.61	−33.32	−38.07	−22.34	$1p\,1/2$	−32.99	−24.39	−26.44	−32.42
$1d\,5/2$	−28.23	−28.32	−33.94	−19.12	$1d\,5/2$	−27.29	−20.74	−21.74	−27.19
$1d\,3/2$	−24.47	−26.05	−30.25	−15.03	$2s\,1/2$	−22.79	−15.98	−17.92	−22.77
$2s\,1/2$	−23.93	−25.36	−29.38	−14.06	$1d\,3/2$	−21.33	−14.73	−18.75	−22.45
$1f\,7/2$	−21.27	−22.91	−25.64	−11.47	$1f\,7/2$	−16.83	−7.92	−14.13	−18.88
$2p\,3/2$	−17.17	−17.67	−20.75	−6.13	$2p\,3/2$	−10.69	−3.58	−9.61	−13.32
$1f\,5/2$	−16.39	−17.65	−21.28	−6.56	$1f\,5/2$	−10.04	−1.08	−7.03	−11.41
$2p\,1/2$	−15.48	−15.,91	−18.75	−4.12	$2p\,1/2$	−9.80	−2.06	−7.54	−10.96
$1g\,9/2$	−14.93	−15.45	−17.59	−2.91	$1g\,9/2$	−7.51	−0.023	−5.98	−9.87
$1g\,7/2$	−9.64	−9.70	−10.70	3.45	$2d\,5/2$	−3.20	2.95	−1.95	−4.02
$2d\,5/2$	−8.97	−8.83	−12.73	1.07	$3s\,1/2$	−2.12	3.85	−1.14	−1.87
$3s\,1/2$	−7.55	−7.10	−9.82	1.15	$2d\,3/2$	−0.11	5.85	−0.39	−0.50
$1h\,11/2$	−7.53	−6.96	−10.37	0.65	$1g\,7/2$			−0.76	
$2d\,3/2$	−7.15	−6.70	−9.55	4.15	$1h\,11/2$			−0.31	
$2f\,7/2$	−2.50	−1.57	−3.57	8.75	$3p\,3/2$			1.35	
$1h\,9/2$	−1.49	0.25	−1.25	12.05	$2f\,7/2$			4.75	
$3p\,3/2$	−1.36	0.65	−2.11	10.45	$3p\,1/2$			5.35	
$3p\,1/2$	−0.59	1.15	−1.11	11.95	$1h\,9/2$			7.65	
$1i\,13/2$	−0.25	−0.14	−2.40	10.15	$1i\,13/2$			7.85	
$3d\,5/2$	2.35				$2f\,5/2$			8.15	
$2g\,9/2$	3.65								
$2g\,7/2$	6.35								
$2f\,5/2$	8.05	0.45	−0.96	11.25					
$1i\,11/2$	9.65								
$3d\,3/2$	15.35								

The low-lying collective phonons (listed in Table 1 for the various nuclei considered) which are taken into account in the $1p\,1h\otimes$ *phonon* coupling have been calculated within RPA using the following known Landau-Migdal parameters

$$f_{in}=-0.002,\quad f'_{ex}=2.30,\quad f'_{in}=0.76$$
$$g=-0.05,\quad g'=0.96,\quad C_0=300\ \text{MeV fm}^3 \qquad (8)$$

for all nuclei. Since the spin-dependent contributions to the low-lying phonon spectrum is small, the difference between $g'=0.86$ and $g'=0.96$ has no noticeable consequences for the results. The parameter f_{ex} has been fitted to available phonon energies and ranges from -5.0 to -3.5 which is not far from the value $f_{ex}=-3.74$ used earlier [12, 13, 15].

The single-particle states have been calculated from

Table 3. Characteristics of $M1$ excitations (E_{is}, E_{iv}, $\bar{E}$ are given in MeV, $B(M1)\uparrow$ and $\sum B(M1)\uparrow$ in μ_0^2)

	$1p\,1h$+cont.				$1p\,1h+2p\,2h$+cont. without $2p\,2h$ GSC				$1p\,1h+2p\,2h$+cont. with $2p\,2h$ GSC				Experiment			
	E_{is}	$B(M1)\uparrow$	E_{iv}	$\sum B(M1)\uparrow$ (interval)	E_{is}	$B(M1)\uparrow$	$\bar{E}$	$\sum B(M1)\uparrow$ (interval)	E_{is}	$B(M1)\uparrow$	$\bar{E}$	$\sum B(M1)\uparrow$ (interval)	E_{is}	$B(M1)\uparrow$	E_{iv} or $\bar{E}$	$B(M1)\uparrow$ or $\sum B(M1)\uparrow$ (interval)
^{48}Ca Figs. 1, 7			10.68	8.64 (~10.68)			$E_{iv}=$ 10.35	6.55 (~10.35) 8.24 (9–19)			$E_{iv}=$ 10.36	6.12 (~10.36) 9.68 (9–19)			$E_{iv}=$ 10.32	3.9±0.3 [31] 5.3±0.6 [31] (7.7–12.7)
^{208}Pb Fig. 2	5.63	0.49	7.97	18.16 (~7.97) (5–15.5)	5.72	0.84	7.66	11.87 (6.3–8.7) 1.41 (8.7–9.9) 4.98 (9.9–15.5) 19.09 (5.0–15.5)	5.72	0.84	7.74	11.57 (6.3–8.7) 2.2 (8.7–9.9) 8.02 (9.9–15.5) 22.6 (5.0–15.5)	5.85 5.85 5.85 6.24	1.6±0.5 [33] $1.01^{+0.42}_{-0.13}$ [32] $1.9^{+0.7}_{-0.4}$ [28]	7.3	≈15.6 [28] (6.7–8.4)
^{56}Ni Figs. 3, 8	6.56	0.31	10.12	11.31 (~10.12) 11.43 (5.5–15) 11.73 (6–45)	6.7	0.24	9.93	4.8 (8.5–11.0) 5.58 (11–15) 10.62 (5.5–15)	6.7	0.24	10.02	5.5 (8.5–11.0) 5.94 (11–15) 11.68 (6–15)				
^{78}Ni Figs. 4, 9	5.88	0.66	10.16	16.0 (~10.16) 16.7 (6.5–15)	6.12	0.64	9.3	10.2 (8.5–10.2) 6.8 (10.2–15.0) 17.64 (5.5–15)	6.12	0.64	9.3	9.5 (8.5–10.2) 7.6 (10.2–15.0) 17.74 (5.5–15)				
^{100}Sn Fig. 5	6.8	1.5	10.15	14.1 (~10.15) 15.6 (6–13)	6.5 6.78 ($\bar{E}=$ 6.67)	0.3 1.4	8.9 9.77 10.5 ($\bar{E}=$ 10.0)	1.3 (7–9.4) 6.6 (9.4–10.15) 3.2 (10.15–10.7) 3 (10.7–13) 15.8 (6–13)								
^{132}Sn Figs. 6, 10	5.8	0.4	8.78	19.0 (~8.78) 19.6 (5.5–15)	5.8	0.4	8.45	13.2 (~8.45) 6.0 (9–15) 19.2 (5.5–15)								

a standard Woods-Saxon potential [24]. To get good agreement with measured single-particle energies which are available for ^{48}Ca, ^{208}Pb, ^{56}Ni [25], ^{132}Sn [25, 26] and, to some extent, for ^{100}Sn [25, 27] the well depth of the central part of the potential has been adjusted, changing the depth parameter by less than 5%. A list of single-particle energies, thus obtained, is given in Table 2. Another check is the energy of the $g_{9/2}(p) \rightarrow g_{7/2}(n)$ Gamow-Teller transition in ^{100}Sn. We find a transition energy of 7.6 MeV which coincides with the results of [27].

As mentioned above, the coupling of single-particle states to phonons gives a contribution to the observed single-particle energies. When adjusting the Woods-Saxon potential to empirical energies such contributions are already accounted for. In order to avoid double counting the particle-phonon contributions should be removed. This leads to a "refined" basis $\{\tilde{\phi}_\lambda, \tilde{\varepsilon}_\lambda\}$. The corrected energies $\tilde{\varepsilon}_\lambda$ are obtained by solving the non-linear equations

$$\tilde{\varepsilon}_\lambda = \varepsilon_\lambda - \mathscr{M}_{\lambda\lambda}(\varepsilon_\lambda) = \varepsilon_\lambda - \frac{1}{2j+1} \sum_{s,\lambda'} |\langle \lambda | g_s | \lambda' \rangle|^2 \left\{ \frac{1-n_{\lambda'}}{\varepsilon_\lambda - \tilde{\varepsilon}_{\lambda'} - \omega_s} + \frac{n_{\lambda'}}{\varepsilon_\lambda - \tilde{\varepsilon}_{\lambda'} + \omega_s} \right\} \tag{9}$$

where $\lambda \equiv \{n, l, j\}$.

Finally, in order to account for instrumental resolution in the experiment we have included an energy averaging parameter Δ.

4. Results and discussion

The results of our calculations are presented in Table 3 and in Figs. 1–10. The continuum RPA results are denoted by $1p\,1h + continuum$ while $1p\,1h + 2p\,2h + continuum$ indicates the results including the $1p\,1h \otimes phonon$ contributions. To elucidate the role of the additional ground state correlations we quote results with and without ($gs(\pm)$) in the figures. The mean energies listed in Table 3 are defined as

$$\bar{E} = \frac{\sum_i E_i B_i(M1\uparrow)}{\sum_i B_i(M1\uparrow)}. \tag{10}$$

Figure 1 shows the calculated strength distribution for ^{48}Ca. In the continuum RPA (dotted line) this is dominated by the $1f_{7/2}(n) \rightarrow 1f_{5/5}(n)$ transition. After inclusion of more complicated configurations the measured centroid energy of 10.23 MeV is quite well reproduced ($\bar{E}^{th} = 10.36$ MeV) while the calculated transition strength is somewhat larger than in the experiment. The additional ground state correlations have no noticeable effect. In ^{208}Pb the two particle-hole transitions

$$1h_{11/2}(p) \rightarrow 1h_{9/2}(p) \quad \text{and} \quad 1i_{13/2}(n) \rightarrow 1i_{11/2}(n)$$

form an isoscalar and isovector transition within the RPA. Taking into account the more complex configurations we obtain reasonable agreement with experiment

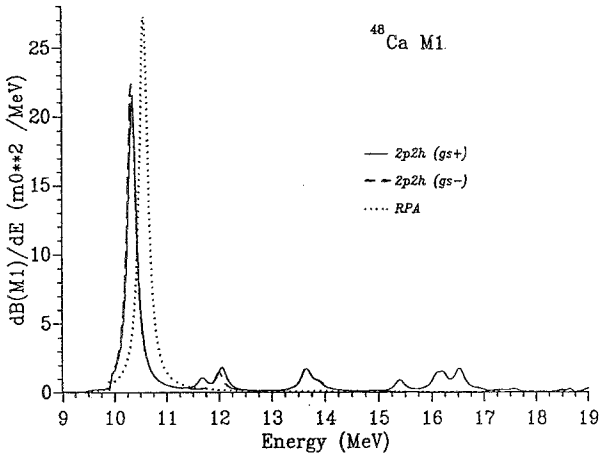

Fig. 1. The $M1$ strength function for ^{48}Ca with an averaging parameter $\Delta = 100$ keV

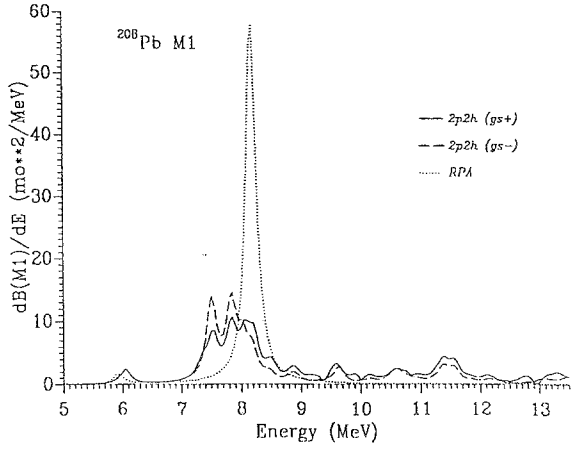

Fig. 2 Same as in Fig. 1 but for ^{208}Pb

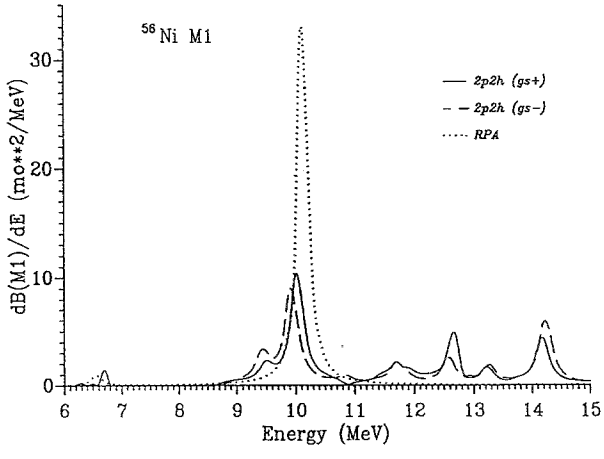

Fig. 3. Same as in Fig. 1 but for ^{56}Ni

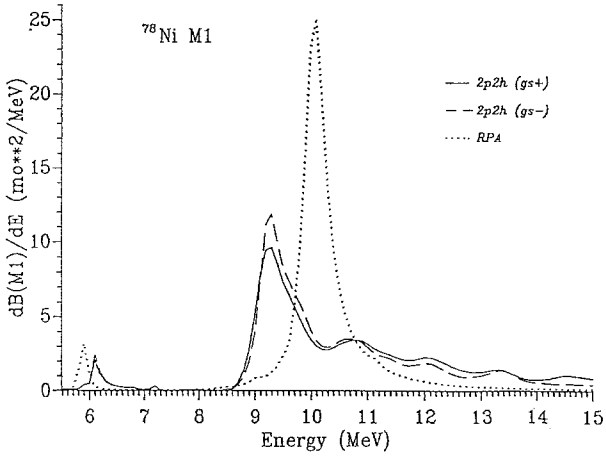

Fig. 4. Same as in Fig. 1 but for ^{78}Ni

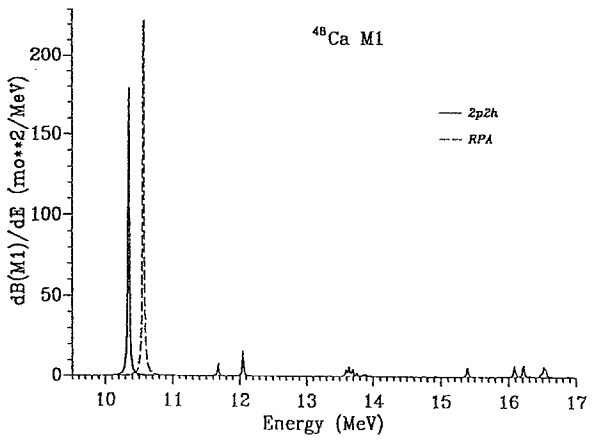

Fig. 7. The $M1$ strength function for ^{48}Ca, $\Delta = 10$ keV

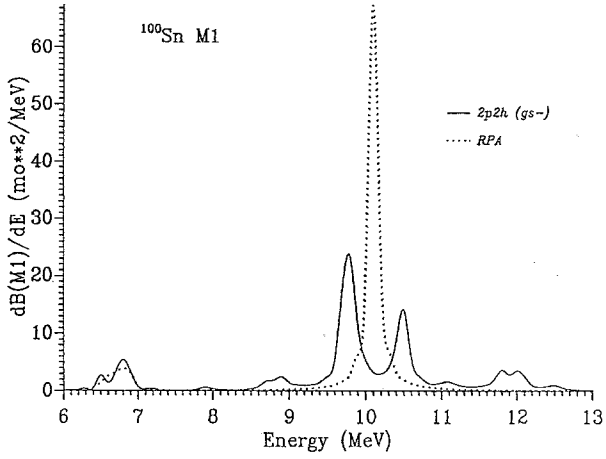

Fig. 5. Same as in Fig. 1 but for ^{100}Sn

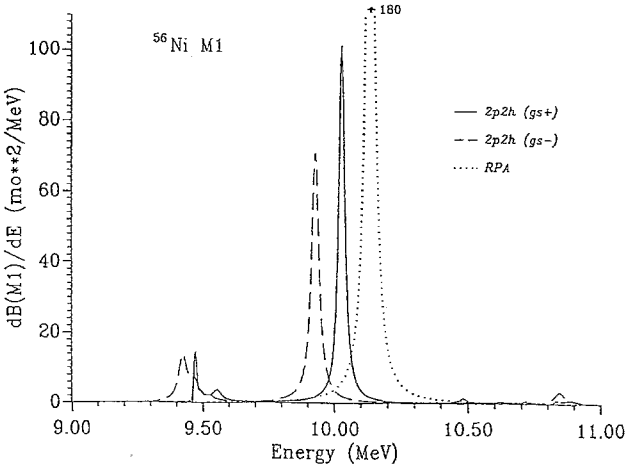

Fig. 8. The $M1$ strength function for ^{56}Ni, $\Delta = 20$ keV

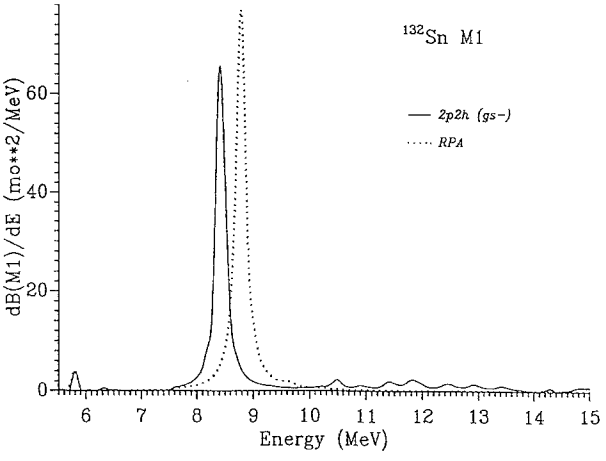

Fig. 6. Same as in Fig. 1 but for ^{132}Sn

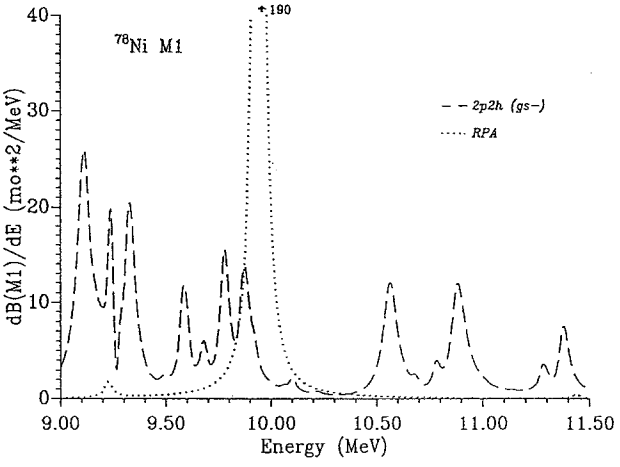

Fig. 9. The $M1$ strength function for ^{78}Ni, $\Delta = 20$ keV

for both the isoscalar 1^+ level at $E_{exp} = 5.85$ MeV and for the isovector $M1$ resonance (Fig. 2). A rather strong quenching has been obtained so that our value $\sum B(M1\uparrow) = 11.6\,\mu_0^2$ is less than the experimental value of $15.6\,\mu_0^2$ [28]. The calculated centroid energy ($\bar{E}^{th} = 7.74$ MeV) is slightly above the measured one ($\bar{E}^{ex} = 7.3$ MeV). The width which can be deduced from Fig. 2 is in good agreement with the experimental value of ~ 1 MeV. The effect of additional GSC is more pronounced than in ^{48}Ca: it increases the strength in the energy interval 9.9–15.5 MeV by about $3\,\mu_0^2$ (see Table 3).

Table 3 and Fig. 3 give the results for ^{56}Ni [3]. As

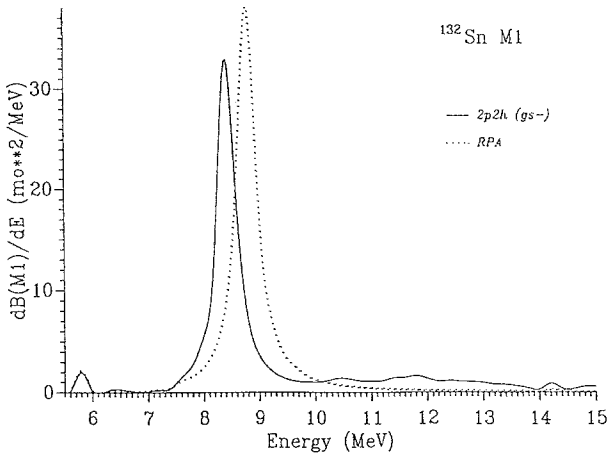

Fig. 10. The $M1$ strength function for ^{132}Sn, $\Delta = 250$ keV

with ^{208}Pb this is a non-spin saturated nucleus with the $1f_{7/2}$ shell filled for protons and neutrons. Thus an isoscalar and isovector state can be formed. The influence of the $1p\,1h \otimes phonon$ states is quite noticeable reducing the strength in the peak by more than a factor of two. As can be seen from Fig. 3 and, in particular, from Fig. 8 (here the averaging parameter is 20 keV only) there is no fragmentation width for the resonance peak. The latter result also seems to hold for ^{132}Sn (Figs. 6, 10). For ^{56}Ni we can compare our results to the continuum RPA calculation of [29]. In these calculations an isoscalar state at 7.5 MeV with $B(M1\uparrow) = 0.4\mu_0^2$ was found which should be compared to 6.6 MeV and $B(M1\uparrow) = 0.3\mu_0^2$ (see Table 3) obtained from $1p\,1h + cont.$ The differences in excitation energy can be traced back to a slight difference in proton single-particle energies as well as a different value of the Landau-Migdal parameter g. While in the present work a value $g = -0.05$ was adopted, [29] uses $g = 0.1$. For the isovector state [29] gives an excitation energy of 9.6 MeV and a transition strength of $B(M1\uparrow) = 9.5\mu_0^2$. This is to be compared to 10.1 MeV and $B(M1\uparrow) = 11.3\mu_0^2$ (see Table 3). The discrepancy in excitation energy comes chiefly from the different choice of the Landau-Migdal parameter $g' = 0.75$ in [29] as compared to $g' = 0.96$ used in the present work. The differences in transition strength are due to different values for the renormalization constants in the effective $M1$ operator. Given the uncertainties in the parameters of the residual interaction and the $M1$ operator we find the discrepancies between the predictions of the two calculations quite acceptable. There is no experimental information yet on ^{56}Ni. On the other hand, there have been high-resolution (e, e') experiments in ^{58}Ni [30] extracting $M1$ strength. Since the additional two neutrons are not expected to drastically change the overall resonance characteristics we may compare our results to these measurements. Experimentally the centroid of the strength has been located at ≈ 10.2 MeV which is in very good agreement with our final result of 10.0 MeV (see Table 3). The summed transition strength $\sum B(M1\uparrow) = 16.9^{+4.6}_{-3.3}\,\mu_0^2$ from 6–15 MeV is somewhat larger than our value of $11.7\mu_0^2$ in the same interval. We also confirm the experimental finding that the strength is strongly fragmented.

We now come to the "very exotic" nuclei ^{78}Ni and ^{100}Sn. In the former the $1f_{7/2}(p)$ and $1g_{9/2}(n)$ are occupied while in the latter both $1g_{9/2}$ shells are full. As seen in Fig. 4 ^{78}Ni has an asymmetric resonance shape with a width of ~ 1 MeV. The $M1$ resonance in the very neutron deficient ^{100}Sn is split into two major peaks with $\bar{E}_1 = 9.8$ MeV and $\bar{E}_2 = 10.5$ MeV (Fig. 5). The low-lying isoscalar level is spit also. These features are caused by the inclusion of the $1p\,1h \otimes phonon$ configurations and for ^{100}Sn also by the very small value of the proton binding energy $B_p = 2.91$ MeV.

5. Conclusion

Within a microscopic approach which includes the continuum RPA as well as $1p\,1h \otimes phonon$ configurations we have calculated isoscalar and isovector $M1$ excitations in the unstable nuclei ^{56,78}Ni and ^{100,138}Sn. To judge the quality of our predictions we have also given results for the "known" $M1$ excitations in ^{48}Ca and ^{208}Pb. For the latter good agreement with experiment in the centroid energy, the transition strength and the width is obtained. This, together with the fact that we have used known universal parameters for the effective interaction and the local $M1$ charge, gives us confidence that the predictions for the unstable nuclei are realistic.

The location of the isovector $M1$ resonances agrees rather well with the RPA calculations. In all cases studied, we find a considerable influence of the particle-phonon coupling on the width and the strength distributions. As compared with the RPA there is noticeable strength in the high-energy tails and a decrease of strength in the resonance region. The damping effects are particularly pronounced in the extremely neutron rich nucleus ^{78}Ni as well as the neutron deficient ^{100}Sn. We did not find a simple A-dependence of the resonance widths. All these features depend delicately on the interplay between the shell structure and the low-lying vibrational modes.

For approaches, like the one used here, which are based on a phenomenological single-particle scheme and the effective Landau-Migdal interaction it is important to experimentally confirm the results presented here. In particular, it would give reassurance of the universality (A-independence) of the Migdal parameters (5) and (7) and hence would allow to generalize the present approach to non-magic nuclei and to use it for many nuclei far from stability.

This work was supported by the German-Russian exchange program and in part by NSF grant PHY-89-21025. Two of us, S.K. and G.T. express their gratitude for warm hospitality of the IKP at the Forschungszentrum Jülich. Useful discussions with Dr. S. Drożdż and Profs. S. Krewald, F. Osterfeld, A. Richter, P. Ring, K. Sistemich and D. Zawischa are gratefully acknowledged.

References

1. Raman, S., Fagg, L.W., Hicks, R.S.: Electric and magnetic giant resonances in nuclei. Speth, J. (ed.), p. 356. Singapore: World Scientific 1991

2. Kienle, P.: Proc. 1989 Int. Nuclear Physics Conf. Hussein, M.S. (ed.), Vol II, p. 467. Singapore: World Scientific 1990; Kienle, P.: Nucl. Phys. A**538**, 111 (1991)
3. Cruz, M.T.F. da, Chan, Y., Larimer, R.-M., Lesko, K.T., Norman, E.B., Stokstad, R.G., Wietfeldt, F.E., Zlimen, I.: Phys. Rev. C**46**, 1132 (1992)
4. Ring, P., Speth, J.: Phys. Lett. B**44**, 477 (1973)
5. Tkachev, V.N., Borzov, I.N., Kamerdzhiev, S.P.: Sov. J. Nucl. Phys. **24**, 373 (1976)
6. Borzov, I.N., Tkachev, V.N.: Izv. Akad. Nauk. SSSR Ser. Fiz. **41**, 1263 (1977)
7. Borzov, I.N., Tolokonnikov, S.V., Fayans, S.A.: Sov. J. Nucl. Phys. **40**, 732 (1984)
8. Khoa, D.T., Ponomarev, V.Yu., Vdovin, A.I.: Joint Institute for Nuclear Research, Preprint E4-86-198 (1986)
9. Cha, D., Schwesinger, B., Wambach, J., Speth, J.: Nucl. Phys. A**430**, 321 (1984)
10. Kamerdzhiev, S.P., Tkachev, V.N.: Phys. Lett. B**142**, 225 (1984); Z. Phys. A **334**, 19 (1989)
11. Pjatov, N.I., Fayans, S.A.: Sov. J. Part. Nucl. **14**, 401 (1983); Bang, J., Fayans, S.A., Gareev, F.A., Ershov, S.N., Pyatov, N.I.: Nucl. Phys. **440**, 445 (1985)
12. Kamerdzhiev, S., Tertychny, G., Unkelbach, W.: Phys. Lett. B**287**, 293 (1992)
13. Kamerdzhiev, S., Speth, J., Tertychny, G., Tselyaev, V.: Nucl. Phys. A **555**, 90 (1993)
14. Migdal, A.B.: Theory of finite Fermi-systems. New York: Wiley 1967
15. Kamerdzhiev, S., Speth, J., Tertychny, G.: Jülich preprint, KFA-IKP(TH)-1992-26
16. Tselyaev, V.I.: Sov. J. Nucl. Phys. **50**, 780 (1989)
17. Shlomo, S., Bertsch, G.: Nucl. Phys. A**243**, 507 (1975)
18. Saperstein, E.E., Fayans, S.A., Khodel, V.A.: Kurchatov Atomic Energy Institute, Preprint IAE-2580 (1976)
19. Soloviev, V.G.: Theory of complex nuclei. London: Pergamon Press 1976; Soloviev, V.G., Stoyanov, Ch., Vdovin, A.I.: Nucl. Phys. A**288**, 376 (1977)
20. Bortignon, P.F., Broglia, R.A.: Nucl. Phys. A**371**, 405 (1981)
21. Wambach, J., Mishra, V.K., Li, Chu-Hsia: Nucl. Phys. A**380**, 285 (1982)
22. Kamerdzhiev, S.P., Tselyaev, V.I.: Sov. J. Nucl. Phys. **44**, 214 (1986)
23. Bauer, R., Speth, J., Klemt, V., Ring, P., Werner, E., Yamazaki, T.: Nucl. Phys. A**209**, 535 (1973)
24. Chepurnov, V.A.: Sov. J. Nucl. Phys. **6**, 696 (1967)
25. Leander, G.A., Dudek, J., Nazarewicz, W., Nix, J.R., Quentin, Ph.: Phys. Rev. C**30**, 416 (1984)
26. Bjornstad, T., Borge, M.J.G., Blomqvist, J., Dincklage, R.D. von, Ewan, G.T., Hoff, P., Jonson, B., Kawade, K., Kerek, A., Klepper, O., Lövhöiden, G., Mattsson, S., Nyman, G., Ravn, H.L., Rudstam, G., Sistemich, K., Tengblad, O., The Isolde Collaboration: Nucl. Phys. A**453**, 463 (1986)
27. Dobaczewski, J., Nazarewicz, W., Plochocki, A., Rykaczewski, K., Zylicz, J.: Z. Phys. A**329**, 267 (1988)
28. Laszewski, R.M., Alarcon, R., Dale, D.S., Hoblit, S.D.: Phys. Rev. Lett. **61**, 1710 (1988)
29. Migli, E., Drożdż, S., Speth, J., Wambach, J.: Z. Phys. **340**, 111 (1991)
30. Mettner, W., Richter, A., Stock, W., Metsch, B.C., Van Hees, A.G.M.: Nucl. Phys. A**473**, 160 (1987)
31. Steffen, W., Gräf, H.-D., Richter, A., Härting, A., Weise, W., Deutschmann, U., Lahm, G., Neuhausen, R.: Nucl. Phys. A**404**, 413 (1983)
32. Müller, S., Küchler, G., Richter, A., Blok, H.P., Blok, H., Jager, C.W. de, Vries, H. de, Wambach, J.: Phys. Rev. Lett. **54**, 293 (1985)
33. Wienhard, K., Ackermann, K., Bangert, K., Berg, U.E.P., Blastig, C., Naatz, W., Ruckelshausen, A., Rück, D., Sneider, R.K.M., Stock, R.: Phys. Rev. Lett. **49**, 18 (1982)